Hindawi
Journal of Nanomaterials
Volume 2017, Article ID 7676158, 11 pages
https://doi.org/10.1155/2017/7676158

Research Article

Nanocomposites of NR/SBR Blend Prepared by Latex Casting Method: Effects of Nano-TiO_2 and Polystyrene-Encapsulated Nano-TiO_2 on the Cure Characteristics, Physical Properties, and Morphology

Anyaporn Boonmahitthisud,[1] Peeraphong Pokphat,[2] Phasawat Chaiwutthinan,[3] and Saowaroj Chuayjuljit[1]

[1]*Department of Materials Science, Faculty of Science, Chulalongkorn University, Bangkok 10330, Thailand*
[2]*Program of Petrochemistry and Polymer Science, Faculty of Science, Chulalongkorn University, Bangkok 10330, Thailand*
[3]*MTEC, National Science and Technology Development Agency (NSTDA), Thailand Science Park, Khlong Luang, Pathum Thani 12120, Thailand*

Correspondence should be addressed to Anyaporn Boonmahitthisud; anyaporn.b@chula.ac.th

Received 22 November 2016; Accepted 12 March 2017; Published 29 March 2017

Academic Editor: R. Torrecillas

Nanocomposites of 80/20 (w/w) natural rubber (NR)/styrene butadiene rubber (SBR) blend with four loadings of either nanosized titanium dioxide ($nTiO_2$) or polystyrene-encapsulated $nTiO_2$ (PS-$nTiO_2$), ranging from 3 to 9 parts by weight per hundred of rubber (phr), were prepared by latex casting method. The PS-$nTiO_2$ synthesized via in situ differential microemulsion polymerization displayed a core-shell morphology ($nTiO_2$ core and PS shell) with an average diameter of 42 nm. The cure characteristics (scorch time, cure time, and cure rate index), mechanical properties (tensile properties, tear strength, and hardness), thermal stability, glass transition temperature, and morphology of the prepared nanocomposites were quantified and compared. The results showed that the cure characteristics of all the nanocomposites were not significantly changed compared to those of the neat NR/SBR blend. The inclusion of an appropriate amount of either $nTiO_2$ or PS-$nTiO_2$ into the NR/SBR blend apparently improved the tensile strength, modulus at 300% strain, tear strength, hardness, and thermal stability but deteriorated the elongation at break of the nanocomposites. Based on differential scanning calorimetry, the glass transition temperature of all the nanocomposites was similar to that of the neat NR/SBR blend. Moreover, the morphology of the PS-$nTiO_2$-filled rubber nanocomposites fractured surface analyzed by scanning electron microscopy showed an improvement in the interfacial adhesion between the rubber phase and the nanoparticles.

1. Introduction

High-performance elastomeric materials have been produced by developing multicomponent systems in terms of rubber blend and/or rubber nanocomposites [1–16]. Blending of rubbers is an important technique to improve certain properties not inherent in a single rubber, while incorporating an inorganic nanofiller (nanosized filler) even at a very low loading (less than 10 wt%) into rubber matrix by physical mixing has attracted considerable interest for both scientific challenges and industrial applications due to their high-performance properties [2, 4–9, 11–16]. Natural rubber (NR) is one of the most important natural biosynthesis polymers, according to its high elasticity, resilience and mechanical properties, low heat build-up and cost, and good formability [1, 4–9]. NR can exhibit higher tensile and tear strength than synthetic rubbers due to its ability to undergo strain crystallization [1, 6–9]. However, NR suffers from poor weathering, ozone, oil, and thermal resistance because of its nonpolarity and high unsaturation [9, 10]. Consequently, NR is normally modified by simple blending with commercially available rubbers and/or fillers to improve its physical properties, thermal stability, and

end-use performances [1–8, 10]. Styrene butadiene rubber (SBR) is a synthetic copolymer derived from styrene and 1,3-butadiene, which can be commercially produced in a latex form by an emulsion polymerization process [1, 6, 16]. SBR possesses higher crack-initiation resistance, wet grip, abrasion resistance, and aging stability than NR, whereas NR has higher strength and performance at low temperature than SBR [1, 4, 6]. Hence, NR has been blended with SBR to enhance its abrasion resistance, thermal stability, and oxidative stability [1, 4, 6]. In this study, NR was blended with SBR in a latex stage to obtain a finer scale dispersion of these two rubber components without phase separation, flocculation, and mastication [6, 11, 12]. However, the rubbers generally require reinforcing fillers to obtain the desired properties for a variety of applications.

Nowadays, several inorganic nanofillers such as silica [3, 6, 8, 12], organoclay [4, 5], titanium dioxide (TiO_2) [2, 11, 12], halloysite nanotubes [13, 14], carbon nanotubes [15], and other nanomaterials [7, 16] have been exploited for preparing rubber nanocomposites. This is because the nanofillers can offer high stiffness and strength by inhibiting the propagation of cracks and delaying the breakdown of materials, along with an increase in the thermal stability of nanocomposites [2, 4–17]. To achieve the desired properties, the nanofillers must sufficiently disperse in the rubber matrix, as poor dispersion results in deteriorating of the performance properties. Nevertheless, each type of filler affects the final properties of nanocomposites in a different way according to their structural and geometrical characteristics. Among the nanofiller precursors, nanosized TiO_2 ($nTiO_2$) has been widely used as a nonblack filler in the rubber industry due to its special properties such as self-cleaning, nontoxicity, photovoltaic effect, antibacteria, UV absorber, high-performance properties, and physicochemical stability [12, 17–21], However, $nTiO_2$ particles possess a very high specific surface area with a large number of hydroxyl groups (-OH) on their surfaces, which can cause a strong filler-filler interaction and a high tendency for self-agglomeration when they disperse in rubber matrix [2, 12, 17, 20–26]. The uneven dispersion of $nTiO_2$ leads to the unimproved mechanical properties and thermal stability of the rubber nanocomposites. Thus, a number of efforts have focused on improving the dispersion of $nTiO_2$ in polymer matrix [17, 20, 21]. For this reason, nanofillers surfaces are commonly modified chemically to reduce their agglomeration by increasing the filler-matrix interaction, while simultaneously decreasing the filler-filler interaction [17, 20–25]. Nowadays, encapsulating inorganic nanoparticles by polymer molecules, forming a core-shell structure, has attracted much attention in the nanotechnology according to the change in their surface characteristics and the improved compatibility with polymers in the nanocomposites [6, 19–27]. Moreover, the hybrid nanoparticles can be designed to enhance the mechanical properties, thermal stability, and performance of the nanocomposites by combining the advantages of different materials.

In this study, hybrid nanoparticles comprised of the $nTiO_2$ core and PS shell were synthesized via in situ differential microemulsion polymerization, which is an efficient process that can produce organic-inorganic hybrid nanoparticles with a core-shell morphology of much smaller diameter (<50 nm) than those obtained from the conventional emulsion polymerization, and requires much lower amount of surfactant than that used in the pristine microemulsion polymerization [6, 27, 28]. However, prior to encapsulating, the $nTiO_2$ was modified by a polymerizable silane coupling agent aimed at bonding PS and $nTiO_2$. This is due to the interaction between -OH groups on the $nTiO_2$ surface and methoxy groups of the silane compound. The modified $nTiO_2$ particles were then well dispersed in a styrene monomer, and the process was followed by the in situ differential microemulsion polymerization. The as-prepared hybrid nanoparticles were characterized by means of Fourier transform infrared (FT-IR) spectroscopy, transmission electron microscopy (TEM), and particle size analysis. Finally, the effects of $nTiO_2$ and PS-$nTiO_2$ on the cure characteristics, mechanical properties, thermal stability, glass transition temperature (T_g), and morphology of the 80/20 (w/w) NR/SBR blend nanocomposites were investigated and compared.

2. Experimental Section

2.1. Materials. High ammonia concentrated NR latex (60% dry rubber content, DRC), aqueous solution of potassium oleate (10 wt%) and potassium hydroxide (10 wt%), and aqueous dispersion of sulfur (50 wt%), zinc oxide (50 wt%), zinc diethyl dithiocarbamate (50 wt%), and Wingstay L antioxidant (50 wt%) were supplied by the Rubber Research Institute of Thailand. SBR latex (50.5% DRC) and styrene monomer were obtained from Dow Chemical Co., Ltd. The $nTiO_2$ with average diameter of 20 nm and specific area of 140–180 m^2/g was purchased from Jebsen & Jessen Technology Co., Ltd. Sodium dodecyl sulfate (SDS) provided by Cognis (Thailand) Co., Ltd., and 2,2-azobisisobutyronitrile (AIBN) provided by Siam Chemical Industry Co., Ltd., were used as a surfactant and initiator, respectively. The silane coupling agent, *3*-mercaptopropyl-trimethoxysilane (MPTMS) (Z-6030 silane), was purchased from Dow Corning Co., Ltd. All materials were used as received without further purification.

2.2. Preparation of MPTMS-Modified $nTiO_2$. The MPTMS-modified $nTiO_2$ (MPTMS-$nTiO_2$) was prepared as follows: 4 g of MPTMS was dissolved in 800 mL of distilled water and the pH was then adjusted to 4.5 using acetic acid in a 1000 mL beaker while stirring for a minimum of 30 min until a clear homogeneous solution was formed. The dry $nTiO_2$ (13.4 g) was then added to the as-prepared MPTMS solution with stirring for an hour. Thereafter, the mixture was dried in an oven at 120°C for 12 h.

2.3. Synthesis and Characterization of PS-$nTiO_2$. The PS-$nTiO_2$ was synthesized by in situ differential microemulsion polymerization as follows: distilled water (60 mL), SDS (8 g), AIBN (0.12 g), and the as-prepared MPTMS-$nTiO_2$ (0.4 g) were mixed in a 500 mL Pyrex glass reactor, which was equipped with a double-jacket condenser, a nitrogen (N_2) gas inlet, and a dropping funnel for monomer feeding. The

system was heated up to 70°C with stirring at 200 rpm using a magnetic stirrer under a N_2 atmosphere. Once the temperature reached 70°C, the styrene monomer (22.5 mL) was fed very slowly, in a dropwise manner over a period of 1.5 h. The reaction system was then maintained at 70°C with constant agitation for an additional hour and then cooled down to room temperature.

For characterizations, the obtained nanolatex was precipitated with methanol, filtered by Buchner funnel, washed well with distilled water, and then dried at 60°C for 12 h. The conversion of monomer (% conversion), solid content (% solid), and yield content (% yield) of the prepared PS-nTiO_2 were measured by gravity method and calculated by the following equations:

$$\%\ \text{conversion} = \frac{(w_0 - w_1)}{w_2} \times 100,$$
$$\%\ \text{solid} = \frac{w_0}{w_3} \times 100, \quad (1)$$
$$\%\ \text{yield} = \left[\frac{(w_0/w_3)}{(w_2/w_4)}\right] \times 100,$$

where w_0, w_1, w_2, w_3, and w_4 are the weights (g) of PS-nTiO_2, nTiO_2, styrene monomer, nanolatex, and mixture, respectively.

The particle size and distribution of the prepared PS-nTiO_2 particles were investigated using a dynamic light scatter analyzer (DLS) with a Nano-series ZX analyzer.

The morphology of the nTiO_2 and PS-nTiO_2 was observed from the TEM images obtained from a Jeol JEM-2100 instrument operated with an acceleration voltage of 80 kV. The sample was stained with 1% (w/v) uranyl acetate for obtaining sufficient contrast.

Functional groups of the samples (nTiO_2, MPTMS-nTiO_2, and PS-nTiO_2) were analyzed from the FT-IR spectra obtained from the Nicolet 6700 over a frequency range of 4000 to 400 cm^{-1}.

2.4. Preparation and Characterization of Rubber Nanocomposites. The NR and SBR lattices were mixed with curing ingredients (potassium oleate, potassium hydroxide, sulfur, zinc oxide, and zinc diethyl dithiocarbamate) and Wingstay L at an ambient temperature according to the recipe (based on dry weight) given in Table 1 and stirred at 150 rpm using a mechanical stirrer for 30 min. The obtained rubber blend was then mixed with either nTiO_2 or PS-nTiO_2 at 3, 5, 7, and 9 phr (based on dry weight) under constant agitation at 150 rpm for 30 min. The homogeneous latex was then kept overnight under mild stirring at 60 rpm for maturation. The obtained nanolatex was then cast as a sheet with a uniform thickness ($20 \times 20 \times 0.15\ cm^3$) on a glass mold, allowed to air-dry for 24 h, and subsequently cured in an oven at 110°C according to the cure time (t_{90}) obtained from the moving die rheometer (MDR; A0225-rheo Tech MD$^+$, Techpro) at 110°C with the rotating speed at 2 rpm. The obtained MDR rheographs also presented t_{s2} (time for incipient cure), and the curing rate index (CRI) was then calculated from the following equation [1, 5, 7]:

$$\text{CRI} = \frac{100}{(t_{90} - t_{s2})}. \quad (2)$$

Table 1: Formulation of the sulphur-curing system for the rubber compound (based on dry weight).

Ingredients	Amount (phr)
NR latex (60% DRC)	80
SBR latex (50.5% DRC)	20
Potassium oleate solution (10% w/v)	0.2
KOH solution (10% w/v)	0.5
ZDEC dispersion (50% w/v)	1.0
Sulfur dispersion (50% w/v)	1.5
Wingstay L dispersion (50% w/v)	1.0
ZnO dispersion (50% w/v)	1.0

The tensile test of the samples was carried out at an ambient temperature according to the ASTM D412 standard using an Instron testing machine (Series 5843) with a load cell of 1 kN and at a crosshead speed of 500 mm/min on the standard dumbbell-shaped specimen. At least five specimens were tested to obtain the average value for the tensile strength, modulus at 300% strain (M300), and elongation at break.

The tear strength was measured according to the ASTM D624 (die C) on an angle-shaped sample using the same Instron testing machine at a strain rate of 500 mm/min. At least five specimens were tested to obtain the average value.

Hardness was measured according to the ASTM D2240 using a durometer (Shore Instrument & Mfg. Co.) and expressed as Shore A hardness.

The thermal stability of the samples was evaluated by thermogravimetric analysis (TGA) on a Perkin Elmer Pyris 1 TGA instrument under a N_2 atmosphere at a heating rate of 20°C/min over the temperature range of 50–800°C. The thermograms displayed the temperatures for onset (T_{onset}), end set ($T_{end\ set}$), 50% weight loss ($T_{50\%}$), and maximum decomposition (T_{max}) and % char.

The T_g of the samples was examined by differential scanning calorimetry (DSC, Mettler Toledo DSC 1 STAR^e) during the second heating scan from −70°C to 10°C under a N_2 atmosphere at a constant heating rate of 5°C/min.

The morphology of the cryogenic fractured surface (in liquid N_2) was observed using scanning electron microscopy (SEM; Jeol JSM-6480LV) under an accelerated voltage of 15 kV with a magnification of 500x. The fractured surface was sputter coated with a thin layer of gold under vacuum prior to analysis.

3. Results and Discussion

The obtained PS-nTiO_2 prepared by in situ differential microemulsion polymerization had the calculated % conversion, % solid, and % yield of about 94%, 22%, and 96%, respectively. The particle size distribution of the prepared PS-nTiO_2, as

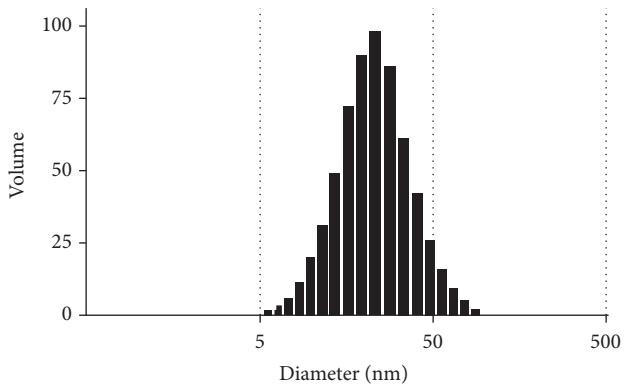

Figure 1: Particle size distribution of the PS-nTiO_2 prepared via in situ differential microemulsion polymerization.

obtained from the DLS analyzer, revealed a unimodal particle size distribution in which most of the particles fall within 17–86 nm diameter range and a mean nanoparticle diameter of 42 nm (Figure 1).

Figure 2 shows representative TEM images of the bare nTiO_2 and PS-nTiO_2 particles. The nTiO_2 particles had an irregular but approximately spherical shape with a high degree of agglomeration (Figure 2(a)), due to the large surface area of nTiO_2 particles and the -OH groups on their surfaces as previously mentioned. In contrast, the core-shell structure (Figure 2(b)) with nTiO_2 particles (dark phase) as a core and PS (grey phase) as a shell can be observed after surface modification, suggesting that the nTiO_2 were successfully encapsulated by PS via the in situ differential microemulsion polymerization. It is assumed that the PS shell effectively suppressed or hindered the agglomeration of the hybrid nanoparticles. However, the encapsulation could be confirmed by analyzing the chemical structures of nTiO_2 and then compared with those of the PS-nTiO_2 using FT-IR analysis.

Figure 3 represents the FT-IR spectra of nTiO_2, MPTMS-nTiO_2, and PS-nTiO_2 in the range of 4000–400 cm^{-1}. The peak at 3309 cm^{-1} shown in the spectrum of nTiO_2 (Figure 3(a)) was contributed to the stretching and bending vibration of the -OH groups on the surface of the nTiO_2 particles, which were active sites for the reaction with methoxy groups of the MPTMS [19, 21, 23, 24], while the broad peak at around 665 cm^{-1} was assigned to the vibration absorption peak of Ti-O and Ti-O-Ti bonds [19, 21, 23, 24]. By contrast, the additional peaks at 2923, 1726, 1641, 1138, and 1037 cm^{-1} seen in the spectrum of MPTMS-nTiO_2 (Figure 3(b)) corresponded to the stretching vibration of C-H, C=O, C=C, Si-O, and Ti-O-Si bonds, respectively [19–21, 24–26], indicating the binding of methoxy groups in MPTMS to the -OH groups on the nTiO_2 surfaces to introduce double bonds onto the nTiO_2 surfaces, which can further react with the styrene monomer. For the PS-nTiO_2 (Figure 3(c)), the FT-IR spectrum shows the characteristic peaks of PS at 3024 (C-H arom), 2917 and 2850 (-CH_2-CH_2), 1596 (C=C arom), 1492 and 1448 (-C_6H_5), and 908 and 698 (-CH= arm) cm^{-1}, while the peaks at 1068 and 543 cm^{-1} were due to the vibration of Ti-O-Si and Ti-O-Ti bonds, respectively [19, 21, 23, 24, 26, 27], indicating the existence of PS on the nTiO_2 particle surface. This confirmed the encapsulation of nTiO_2 particles by PS with the aid of MPTMS coupling agent through the free radical copolymerization of styrene monomers with methacrylate groups of MPTMS that chemically bonded with the nTiO_2 core via in situ differential microemulsion polymerization.

t_{s2} and t_{90} obtained from the MDR rheographs and the CRI of the 80/20 (w/w) NR/SBR blend and its nanocomposites filled with 3, 5, 7, or 9 phr of the respective nanoparticle fillers (nTiO_2 and PS-nTiO_2) are summarized in Table 2. t_{s2} is a measure of the time to premature vulcanization while t_{90} is the optimum cure time of the vulcanizates. It can be seen that t_{s2} of all the nanocomposites was almost the same as that of the neat 80/20 (w/w) NR/SBR blend, indicating that the inclusion of either nTiO_2 or PS-nTiO_2 at a very low loading showed a little or no effect on t_{s2} of the nanocomposites. For the nTiO_2-filled rubber nanocomposites, t_{90} increased by 3.2 and 3.6 min with increasing TiO_2 contents to 3 phr and 5 phr, respectively, compared to that of the neat NR/SBR blend. This is attributed to the absorption of accelerator by the -OH groups on the nTiO_2 surface, which consequently lowered the accelerator activity and slowed down the sulfur vulcanizing reaction, resulting in the delayed t_{90} of the nanocomposites [15, 29]. The existence of the surface -OH groups was previously confirmed by the FT-IR analysis. However, at higher loading levels of nTiO_2 (7 and 9 phr), the t_{90} values gradually decreased owing to the agglomeration of the nTiO_2 that covered some of the -OH groups and so lowered the amount of accelerator absorption. For the PS-nTiO_2-filled rubber nanocomposites, t_{90} was slightly longer (1.7–2.9 min) than that of the neat NR/SBR blend and did not change significantly with increasing PS-nTiO_2 contents. In addition, the nTiO_2-filled rubber nanocomposites exhibited a higher increase in t_{90} than the PS-nTiO_2-filled rubber nanocomposites when compared at the same filler loading. This may be due to the PS shell that masked some of the -OH groups and also lowered the amount of accelerator absorption. The CRI of all the nanocomposites was slightly lower than that of the neat NR/SBR blend (Table 2), again due to the accelerator absorption by the nanofillers as previously mentioned.

3.1. Mechanical Properties. The experimental data related to the mechanical properties (tensile strength, M300, elongation at break, tear strength, and hardness) of the 80/20 (w/w) NR/SBR blend and its nanocomposites filled with 3, 5, 7, and 9 phr of the respective nanoparticle fillers (nTiO_2 and PS-nTiO_2) are shown in Figures 4–6 and Table 3. It can be observed that all the nanocomposites have higher tensile strength, M300, tear strength, and hardness and lower elongation at break than the neat blend. This may be due to the reinforcing capability of nTiO_2 and PS-nTiO_2 caused by the binding force generated between the interface of nanoparticles and rubber matrix. The tensile strength of neat NR/SBR blend was 24.9 MPa. For the nTiO_2-filled rubber nanocomposites, the tensile strength increased to the highest value (35.5 MPa) at 5 phr of nTiO_2, which was 42.6% increase. The increased tensile strength was achieved because the nTiO_2 were finely dispersed in the rubber matrix and the stress was highly transferred across the interface of the nTiO_2 and

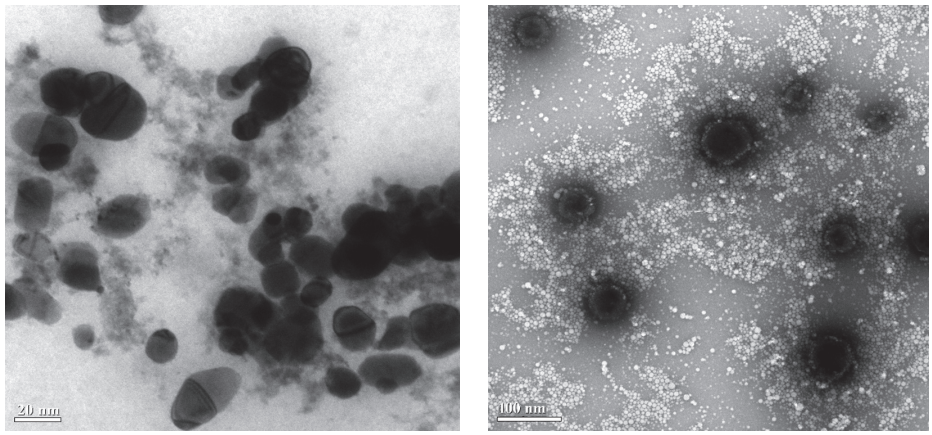

(a) (b)

Figure 2: Representative TEM images of (a) bare $nTiO_2$ and (b) PS-$nTiO_2$.

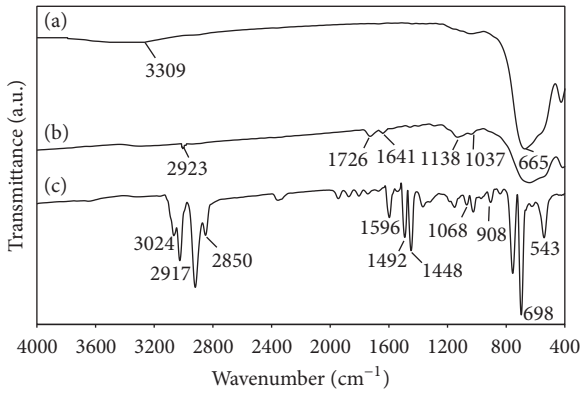

Figure 3: FT-IR spectra of (a) $nTiO_2$, (b) MPTMS-$nTiO_2$, and (c) PS-$nTiO_2$.

Table 2: Cure characteristics of the rubber compounds.

Composition	t_{S2} (min)	t_{90} (min)	CRI (%·min^{-1})
NR/SBR (wt%/wt%)			
80/20	1.1	23.6	4.4
NR/SBR/$nTiO_2$ (wt%/wt%/phr)			
80/20/3	1.2	26.8	3.9
80/20/5	1.5	27.2	3.9
80/20/7	1.5	26.3	4.0
80/20/9	1.2	25.5	4.1
NR/SBR/PS-$nTiO_2$ (wt%/wt%/phr)			
80/20/3	1.2	26.5	4.0
80/20/5	1.2	26.0	4.0
80/20/7	1.2	25.9	4.1
80/20/9	1.2	25.3	4.2

NR/SBR matrix. However, the tensile strength was considerably decreased to 27.5 MPa upon addition of $nTiO_2$ at 7 phr and then slightly decreased to 26.3 MPa at 9 phr (Figure 4(a)). This may be attributed to the self-agglomeration of $nTiO_2$ particles at high loadings that then lowered the filler-rubber interaction. In contrast, the tensile strength of the PS-$nTiO_2$-filled rubber nanocomposites increased up to the highest value of 36.7 MPa (47.4% increase) at 3 phr of PS-$nTiO_2$, followed by the substantial decrease to 28.5, 27.2, and 26.2 MPa at 5, 7, and 9 phr, respectively. The initial increment in the tensile strength at 3 phr filler was due to the PS molecules on the $nTiO_2$ surfaces that improved not only the dispersion of $nTiO_2$ particles but also the filler-rubber interfacial adhesion by chain entanglement of PS molecules of the PS-$nTiO_2$ particles and the SBR, which give rise to the additional crosslinks in the network structure that tend to hold themselves tightly. Thereafter, a reduction in the tensile strength at higher loading levels of PS-$nTiO_2$ (5–9 phr) may be due to the self-agglomeration of the excess PS-$nTiO_2$ particles located at the phase boundary of NR and SBR (because the PS-$nTiO_2$ particles were concentrated in the SBR phase), resulting in an incomplete network structure and poor crosslinking across the NR and SBR phase boundary. Similar trend was also observed for the tear strength as discussed later.

All nanocomposites containing the respective nanoparticle filler ($nTiO_2$ and PS-$nTiO_2$) exhibited a dose-dependent increase in the M300 over that of the neat 80/20 (w/w) NR/SBR blend with increasing filler levels (3–9 phr) from 3.5 MPa of the neat blend to 4.1–5.7 MPa (17–62.8% increase) for $nTiO_2$ and 4–4.9 MPa for PS-$nTiO_2$ (14.3–40% increase) (Figure 4(b)). This suggests that the incorporation of nanofillers even at a very low content can effectively reduce the mobility of rubber chains and increase the stiffness of the resulting nanocomposites. However, the increased M300 induced by the addition of $nTiO_2$ was slightly higher than that induced by the inclusion of PS-$nTiO_2$. This could be because the PS-$nTiO_2$-filled rubber nanocomposites possessed lower $nTiO_2$ content than the $nTiO_2$-filled rubber nanocomposites when compared at the same nanofiller loadings. In addition, the PS shell could provide higher free volume in the rubber matrix and thus facilitated the segmental movement.

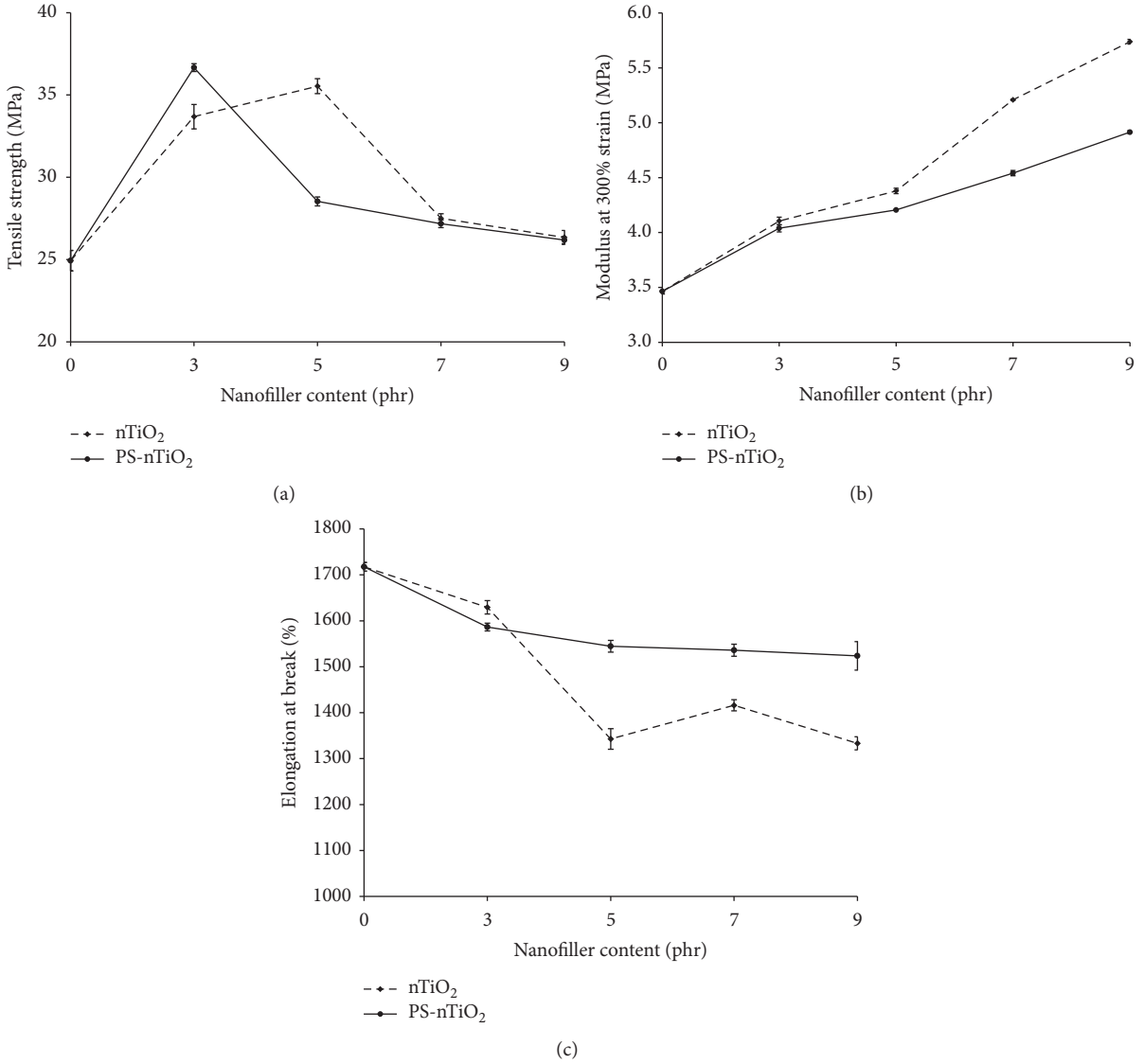

Figure 4: Tensile properties of 80/20 (w/w) NR/SBR blend and its nanocomposites in terms of (a) tensile strength, (b) M300, and (c) elongation at break.

Figure 4(c) shows a decrease in the elongation at break of the 80/20 (w/w) NR/SBR blend with increasing inclusion levels of the respective nanoparticle fillers ($nTiO_2$ and PS-$nTiO_2$). The elongation at break was decreased from 1717.6% of the neat NR/SBR blend to 1333.2–1629.4% (5.1–22.4% decrease) and 1523.6–1586.4% (7.6–11.3% decrease) by the inclusion of 3–9 phr of $nTiO_2$ and PS-$nTiO_2$, respectively. This observation is expected since the stiff nanoparticles would act as restriction sites for the rubber chain movement and so reduce the elongation at break of the nanocomposites. However, the elongation at break of the neat NR/SBR blend is largely retained due to the very low loading of the nanofiller particles, and so the prepared vulcanizates were flexible nanocomposites. In addition, as the nanofiller loading was beyond 3 phr, the elongation at break of the PS-$nTiO_2$-filled rubber nanocomposites was higher than that of the $nTiO_2$-filled rubber nanocomposites when compared at the same filler loading. This could also be due to the lower $nTiO_2$ content and the higher free volume in the matrix of the PS-$nTiO_2$-filled rubber nanocomposites that facilitated the segmental movement as mentioned above.

The tear strength of the 80/20 (w/w) NR/SBR blend and its nanocomposites containing 3–9 phr of $nTiO_2$ and PS-$nTiO_2$ exhibited the same trend with the tensile strength. All the nanocomposites have higher tear strength than the neat blend (Figure 5). The tear strength of the neat NR/SBR blend was about 77.5 N/mm. For the $nTiO_2$-filled rubber nanocomposites, the tear strength increased to a maximum value (121.6 N/mm) at 5 phr, which was about 56.9% higher than that of the neat NR/SBR blend. However, the tear strength considerably decreased to 98 N/mm upon addition of $nTiO_2$ at 7 phr and then slightly decreased to 94.4 N/mm at 9 phr (Figure 5). In contrast, the tear strength of the PS-$nTiO_2$-filled rubber nanocomposites increased up to the highest value of

Table 3: Mechanical properties of 80/20 (w/w) NR/SBR blend and its nanocomposites.

Composition	Tensile strength (MPa)	M300 (MPa)	Elongation at break (%)	Tear strength (N/mm)	Hardness (shore A)
NR/SBR (wt%/wt%)					
80/20	24.9 ± 0.6	3.5 ± 0.02	1717.6 ± 9.4	77.5 ± 7.5	46.7 ± 0.3
NR/SBR/nTiO_2 (wt%/wt%/phr)					
80/20/3	33.7 ± 0.7	4.1 ± 0.04	1629.4 ± 14.6	118.0 ± 1.2	50.3 ± 0.3
80/20/5	35.5 ± 0.5	4.4 ± 0.02	1342.8 ± 22.5	121.6 ± 11.5	53.2 ± 0.3
80/20/7	27.5 ± 0.3	5.2 ± 0.01	1416.5 ± 12.0	98.0 ± 4.8	55.5 ± 0.5
80/20/9	26.3 ± 0.4	5.7 ± 0.02	1333.2 ± 14.2	94.4 ± 6.8	57.7 ± 0.3
NR/SBR/PS-nTiO_2 (wt%/wt%/phr)					
80/20/3	36.7 ± 0.2	4.0 ± 0.03	1586.4 ± 8.4	130.6 ± 7.7	55.7 ± 0.3
80/20/5	28.5 ± 0.3	4.2 ± 0.01	1544.6 ± 12.9	100.7 ± 5.8	56.2 ± 5.8
80/20/7	27.2 ± 0.2	4.5 ± 0.02	1535.9 ± 13.2	85.3 ± 4.1	60.2 ± 0.3
80/20/9	26.2 ± 0.2	4.9 ± 0.02	1523.6 ± 31.1	83.5 ± 6.6	65.5 ± 0.5

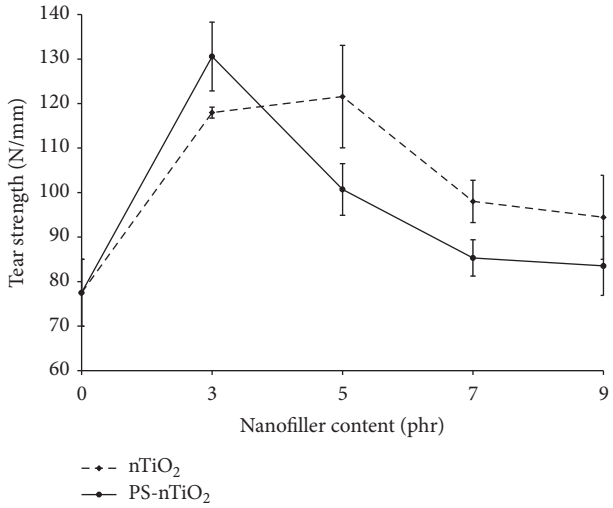

Figure 5: Tear strength of 80/20 (w/w) NR/SBR blend and its nanocomposites.

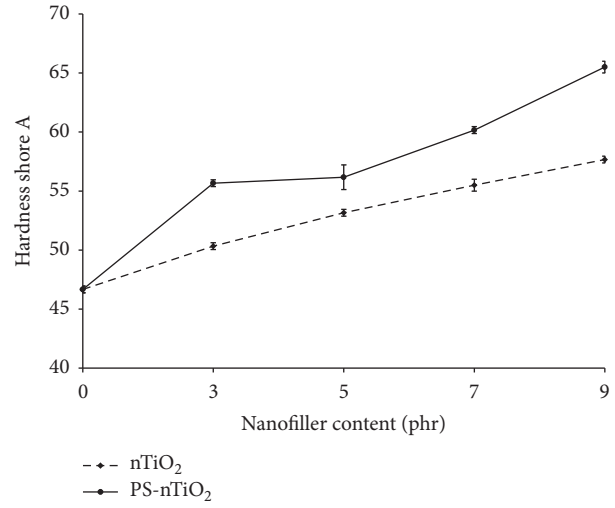

Figure 6: Hardness of 80/20 (w/w) NR/SBR blend and its nanocomposites.

130.6 N/mm (68.5% increase) at 3 phr of PS-nTiO_2, followed by the substantial decrease in the tear strength to 100.7, 85.3, and 83.5 N/mm at 5, 7, and 9 phr, respectively. This may be due to the same reasons as previously discussed in the results of the tensile strength.

Finally, all the nanocomposites exhibited improved hardness as compared to the neat 80/20 (w/w) NR/SBR blend (Figure 6), and the hardness was increased with increasing loading of nanofillers as expected due to the restriction of segmental motion of the rubber chains. The hardness increased from 46.7 Shore A of the neat NR/SBR blend to 50.3–57.7 Shore A (7.7–23.6% increase) and 55.7–65.5 Shore A (19.3–40.3% increase) by the inclusion of 3–9 phr of nTiO_2 and PS-nTiO_2, respectively. As can be seen, the increased hardness induced by the addition of PS-nTiO_2 was much higher than that induced by the inclusion of nTiO_2. This suggested that the nTiO_2 particles were embedded in the rubber matrix, while the PS-nTiO_2 particles can be located on the surface of the nanocomposites.

3.2. Thermal Behaviors. The thermal stability in terms of T_{onset}, $T_{50\%}$, $T_{end\ set}$, T_{max}, and % char of the samples was studied by TG analysis. The representative TGA curves of the 80/20 (w/w) NR/SBR blend and its nanocomposites containing 3, 5, 7, and 9 phr of either nTiO_2 or PS-nTiO_2 are shown in Figure 7 and the degradation temperatures are listed in Table 4. The degradation of all samples occurred in one stage with the maximum weight loss temperature (T_{max}) at around 400°C as obtained from the derivative thermogravimetric (DTG) thermograms (not shown here). This indicated that both nTiO_2 and PS-nTiO_2 had no effect on the degradation mechanism of the NR/SBR blend but only affected the degree of degradation. However, the degradation temperatures revealed that the addition of either nTiO_2 or PS-nTiO_2

Table 4: Thermal characteristics of 80/20 (w/w) NR/SBR blend and its nanocomposites.

Composition	T_{onset} (°C)	$T_{50\%}$ (°C)	$T_{end\ set}$ (°C)	T_{max} (°C)	T_g (°C)
NR/SBR (wt%/wt%)					
80/20	350	409	464	400	−61.1
NR/SBR/nTiO$_2$ (wt%/wt%/phr)					
80/20/3	374	410	465	400	−62.0
80/20/5	377	413	466	400	−62.0
80/20/7	379	414	467	400	−62.2
80/20/9	376	418	470	401	−61.7
NR/SBR/PS-nTiO$_2$ (wt%/wt%/phr)					
80/20/3	375	410	472	400	−61.8
80/20/5	376	410	473	402	−61.9
80/20/7	378	409	474	402	−61.8
80/20/9	375	410	473	398	−62.1

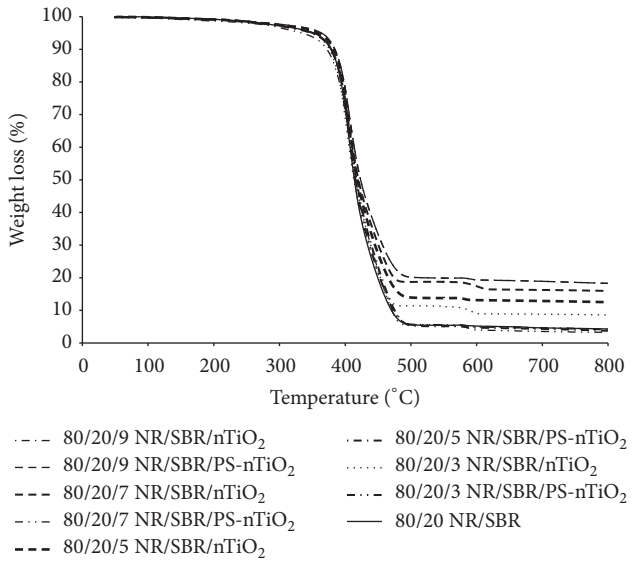

Figure 7: TGA thermograms of 80/20 (w/w) NR/SBR blend and its nanocomposites.

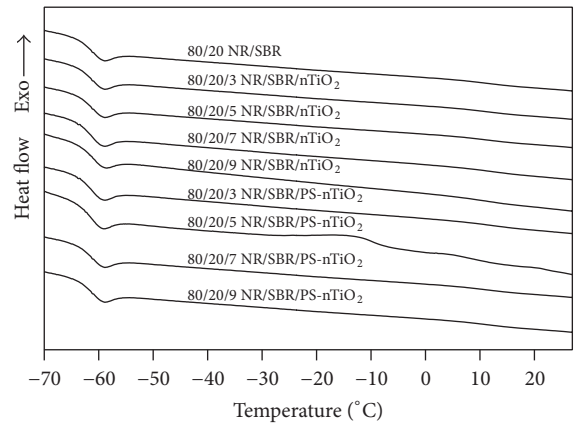

Figure 8: DSC thermograms of 80/20 (w/w) NR/SBR blend and its nanocomposites.

exhibited a dose-dependent increase in the thermal stability over that of the neat NR/SBR blend by shifting T_{onset}, $T_{50\%}$, and $T_{end\ set}$ towards higher temperatures. This behavior may be caused mostly by the binding force between the interface of the nanofillers and rubber matrix and consequently restricted the mobility of the rubber chains. In addition, both nTiO$_2$ and PS-nTiO$_2$ have much higher thermal stability than both NR and SBR, thus consuming some of the heat and acting as a heat barrier in the thermal decomposition process [14, 17, 19, 20]. The nTiO$_2$ lost only 2.1 wt% at 800°C [20]. As expected, the char formation of all the nanocomposites was higher than that of the neat NR/SBR blend (Figure 7). This is because the residue left in the system was mostly inorganic nanofillers. Moreover, the increased char formation may delay and reduce the thermal degradation of the samples by restricting the diffusion of volatile degradation products out of the samples [2, 6, 14, 20].

DSC thermogram of all the samples recorded from the second heating scan (Figure 8) displayed one endothermic peak, associated with T_g. T_g of neat 80/20 NR/SBR was −61.1°C and remained almost constant with the addition of either nTiO$_2$ or PS-nTiO$_2$ (Table 4), suggesting that the presence of nanofillers had very little influence on T_g of the nanocomposites.

3.3. Morphology. The morphology of the 80/20 (w/w) NR/SBR blend and its two nanocomposite series was studied using SEM. Representative SEM images of all the samples are shown in Figure 9. All the images revealed a relatively rough and uneven fractured surface, indicating that the samples failed in a ductile manner, which is in good agreement with the result of the elongation at break. However, the PS-nTiO$_2$-filled rubber nanocomposites exhibited rougher fractured surfaces (Figures 9(f)–9(i)) compared with the neat NR/SBR blend (Figure 9(a)) and the nTiO$_2$-filled rubber nanocomposites (Figures 9(b)–9(e)). This may be due to the better interaction between the PS-nTiO$_2$ particles and the rubber matrix.

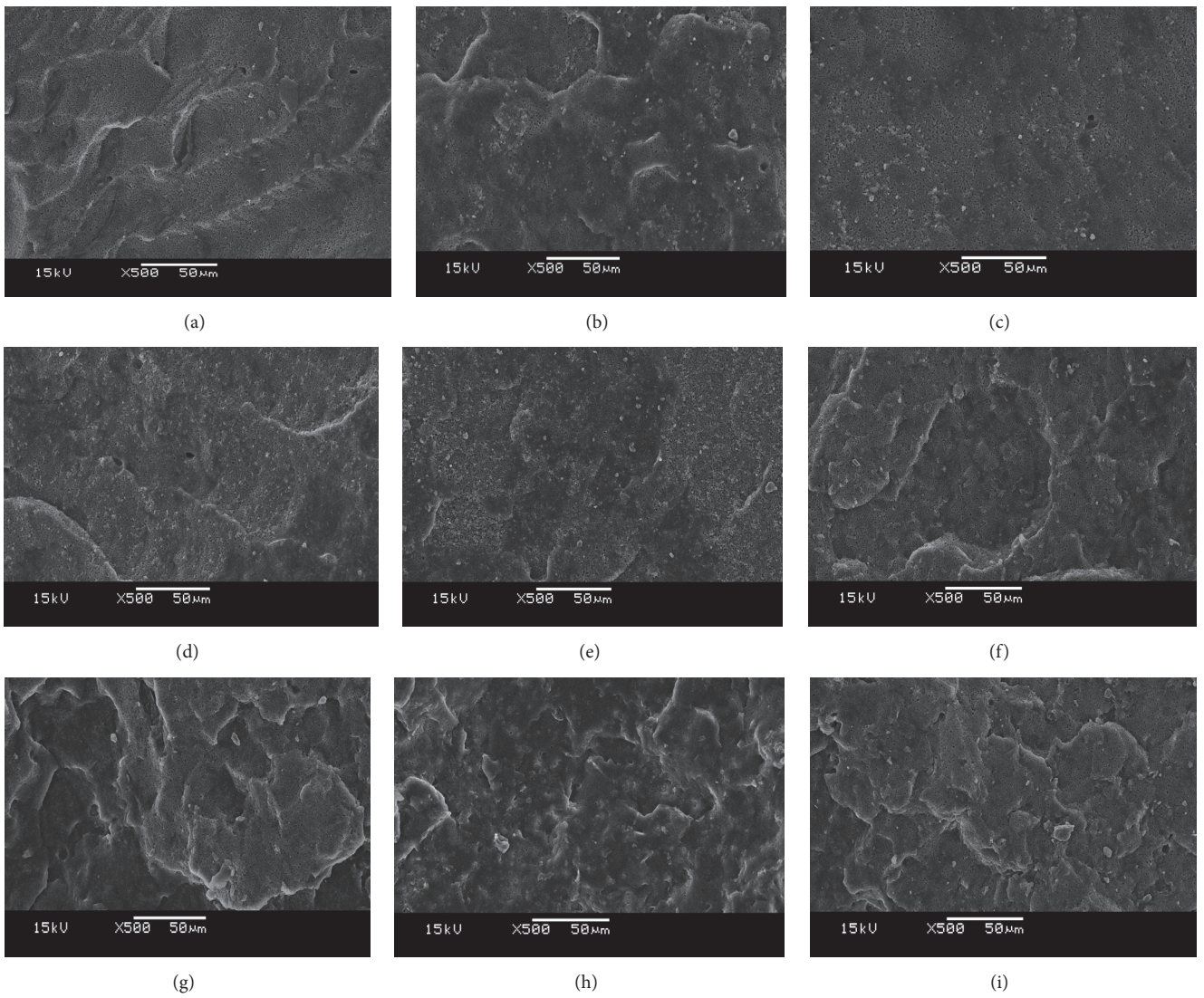

Figure 9: Representative SEM images (×500 magnification) of (a) 80/20 (w/w) NR/SBR blend; (b–e) 80/20 (w/w) NR/SBR blend nanocomposites with $nTiO_2$ at (b) 3 phr, (c) 5 phr, (d) 7 phr, and (e) 9 phr; and (f–i) 80/20 (w/w) NR/SBR blend nanocomposites with PS-$nTiO_2$ at (f) 3 phr, (g) 5 phr, (h) 7 phr, and (i) 9 phr.

4. Conclusions

The $nTiO_2$ was successfully encapsulated by PS via differential microemulsion polymerization. The core-shell structure of PS-$nTiO_2$ was confirmed by FT-IR spectra and TEM image. The synthesized PS-$nTiO_2$ had the calculated % conversion, % solid, and % yield of about 94%, 22%, and 96%, respectively, with average particle size of 42 nm. The selected different loadings (3, 5, 7, and 9 phr) of $nTiO_2$ and PS-$nTiO_2$ were incorporated into 80/20 (w/w) NR/SBR blend through latex compounding method. Their cure characteristics (t_{s2}, t_{90}, and CRI), mechanical properties (tensile properties, tear strength, and hardness), thermal stability (T_{onset}, $T_{50\%}$, $T_{end\ set}$, T_{max}, and % char), T_g, and morphology of the prepared nanocomposites were investigated. The nanofiller addition had no particular influence on the cure characteristics, T_{max} and T_g of all the 80/20 (w/w) NR/SBR blend nanocomposites. However, the presence of an appropriate amount of the nanofillers apparently improved the tensile strength, M300, tear strength, hardness, and thermal stability but deteriorated the elongation at break of the NR/SBR blend nanocomposites. Moreover, the encapsulation of $nTiO_2$ by PS enhanced the compatibility of the $nTiO_2$ in the 80/20 (w/w) NR/SBR blend matrix.

Conflicts of Interest

The authors declare that they have no conflicts of interest.

Acknowledgments

The authors acknowledge the Program of Petrochemistry and Polymer Science and Department of Materials Science,

Faculty of Science, Chulalongkorn University, for financial, material, and instrument support.

References

[1] M. M. Hassan, A. A. Abd El-Megeed, and N. A. Maziad, "Evaluation of curing and physical properties of NR/SBR blends using radiation-grafting copolymer," *Polymer Composites*, vol. 30, no. 6, pp. 743–750, 2009.

[2] T. E. Motaung, A. S. Luyt, and S. Thomas, "Morphology and properties of NR/EPDM rubber blends filled with small amounts of titania nanoparticles," *Polymer Composites*, vol. 32, no. 8, pp. 1289–1296, 2011.

[3] H. H. Le, S. Ilisch, D. Heidenreich, A. Wutzler, and H.-J. Radusch, "Kinetics of the phase selective localization of silica in rubber blends," *Polymer Composites*, vol. 31, no. 10, pp. 1701–1711, 2010.

[4] C. Shan, Z. Gu, L. Wang et al., "Preparation, characterization, and application of NR/SBR/Organoclay nanocomposites in the tire industry," *Journal of Applied Polymer Science*, vol. 119, no. 2, pp. 1185–1194, 2011.

[5] M. Tavakoli, A. A. Katbab, and H. Nazockdast, "NR/SBR/organoclay nanocomposites: effects of molecular interactions upon the clay microstructure and mechano-dynamic properties," *Journal of Applied Polymer Science*, vol. 123, no. 3, pp. 1853–1864, 2012.

[6] A. Boonmahitthisud and S. Chuayjuljit, "Effects of nanosized polystyrene and polystyrene-encapsulated nanosilica on physical properties of natural rubber/styrene butadiene rubber nanocomposites," *Polymer—Plastics Technology and Engineering*, vol. 51, no. 3, pp. 311–316, 2012.

[7] Z. Gu, G. Song, W. Liu et al., "Preparation and properties of styrene butadiene rubber/natural rubber/organo-bentonite nanocomposites prepared from latex dispersions," *Applied Clay Science*, vol. 46, no. 3, pp. 241–244, 2009.

[8] C. M. Vu, H. T. Vu, and H. J. Choi, "Fabrication of natural rubber/epoxidized natural rubber/nanosilica nanocomposites and their physical characteristics," *Macromolecular Research*, vol. 23, no. 3, pp. 284–290, 2015.

[9] S. Chuayjuljit, T. Nutchapong, O. Saravari, and A. Boonmahitthisud, "Preparation and characterization of epoxidized natural rubber and epoxidized natural rubber/carboxylated styrene butadiene rubber blends," *Journal of Metals, Materials and Minerals*, vol. 25, no. 1, pp. 27–36, 2015.

[10] M. Phiriyawirut and S. Luamlam, "Improved automotive fuel resistance of natural rubber/chlorosulfonated polyethylene blends by blending epoxidized natural polymer," *Open Journal of Organic Polymer Materials*, vol. 3, no. 4, pp. 104–109, 2013.

[11] T. M. Arantes, K. V. Leão, M. I. B. Tavares, A. G. Ferreira, E. Longo, and E. R. Camargo, "NMR study of styrene-butadiene rubber (SBR) and TiO_2 nanocomposites," *Polymer Testing*, vol. 28, no. 5, pp. 490–494, 2009.

[12] A. P. Meera, R. Tlili, A. Boudenne et al., "Thermophysical and mechanical properties of TiO_2 and silica nanoparticle-filled natural rubber composites," *Journal of Elastomers and Plastics*, vol. 44, no. 4, pp. 369–382, 2012.

[13] H. Ismail and S. M. Shaari, "Curing characteristics, tensile properties and morphology of palm ash/halloysite nanotubes/ethylene-propylene-diene monomer (EPDM) hybrid composites," *Polymer Testing*, vol. 29, no. 7, pp. 872–878, 2010.

[14] H. Ismail and H. S. Ahmad, "Effect of halloysite nanotubes on curing behavior, mechanical, and microstructural properties of acrylonitrile-butadiene rubber nanocomposites," *Journal of Elastomers and Plastics*, vol. 46, no. 6, pp. 483–498, 2014.

[15] A. M. Shanmugharaj and S. Hun Ryu, "Influence of aminosilane-functionalized carbon nanotubes on the rheometric, mechanical, electrical and thermal degradation properties of epoxidized natural rubber nanocomposites," *Polymer International*, vol. 62, no. 10, pp. 1433–1441, 2013.

[16] S. Mishra, N. G. Shimpi, and U. D. Patil, "Effect of Nano $CaCO_3$ on thermal properties of Styrene Butadiene Rubber (SBR)," *Journal of Polymer Research*, vol. 14, no. 6, pp. 449–459, 2007.

[17] Y. Wu, L. Song, and Y. Hu, "Thermal properties and combustion behaviors of polystyrene/surface-modified TiO_2 nanotubes nanocomposites," *Polymer—Plastics Technology and Engineering*, vol. 51, no. 6, pp. 647–653, 2012.

[18] J. Huang, X. Lu, N. Zhang et al., "Study on the properties of nano-TiO_2/polybutylene succinate composites prepared by vane extruder," *Polymer Composites*, vol. 35, no. 1, pp. 53–59, 2014.

[19] L. G. Bach, M. R. Islam, S. Y. Seo, and K. T. Lim, "A novel route for the synthesis of poly(2-hydroxyethyl methacrylate) grafted TiO_2 nanoparticles via surface thiol-lactam initiated radical polymerization," *Journal of Applied Polymer Science*, vol. 127, no. 1, pp. 261–269, 2013.

[20] S. Mallakpour, F. Zeraatpisheh, and M. R. Sabzalian, "Sonochemical-assisted fabrication of biologically active chiral poly(ester-imide)/TiO_2 bionanocomposites derived from L-methionine and L-tyrosine amino acids," *Express Polymer Letters*, vol. 5, no. 9, pp. 825–837, 2011.

[21] G. Wang, G. Chen, Z. Wei et al., "A comparative study of TiO_2 and surface-treated TiO_2 nanoparticles on thermal and mechanical properties of poly(ε-caprolactone) nanocomposites," *Journal of Applied Polymer Science*, vol. 125, no. 5, pp. 3871–3879, 2012.

[22] K. Matsuyama and K. Mishima, "Preparation of poly(methyl methacrylate)-TiO_2 nanoparticle composites by pseudo-dispersion polymerization of methyl methacrylate in supercritical CO_2," *Journal of Supercritical Fluids*, vol. 49, no. 2, pp. 256–264, 2009.

[23] D.-G. Yu, J. H. An, J. Y. Bae, S. D. Ahn, S.-Y. Kang, and K. S. Suh, "Preparation of titanium dioxide/poly(methyl methacrylate-co-n-butyl acrylate-co-methacrylic acid) hybrid composite particles via emulsion polymerization," *Journal of Applied Polymer Science*, vol. 97, no. 1, pp. 72–79, 2005.

[24] J. Zhang, J. Gao, X. Sun, Z. Peng, and J. Diao, "Preparation and characterization of TiO_2/poly(St-co-MAA) core/shell composite particles," *Iranian Polymer Journal*, vol. 16, no. 1, pp. 39–46, 2007.

[25] M. Yang and Y. Dan, "Preparation and characterization of poly(methyl methacrylate)/titanium oxide composite particles," *Colloid and Polymer Science*, vol. 284, no. 3, pp. 243–250, 2005.

[26] X. Ding, J. Zhao, Y. Liu, H. Zhang, and Z. Wang, "Silica nanoparticles encapsulated by polystyrene via surface grafting and in situ emulsion polymerization," *Materials Letters*, vol. 58, no. 25, pp. 3126–3130, 2004.

[27] S. Chuayjuljit, N. Sukasem, and A. Boonmahitthisud, "Effects of silica, poly(methyl methacrylate) and poly(methyl methacrylate)-grafted-silica nanoparticles on the physical properties of plasticized-poly(vinyl chloride)," *Polymer—Plastics Technology and Engineering*, vol. 53, no. 2, pp. 116–122, 2014.

[28] G. He, Q. Pan, and G. L. Rempel, "Synthesis of poly(methyl methacrylate) nanosize particles by differential microemulsion polymerization," *Macromolecular Rapid Communications*, vol. 24, no. 9, pp. 585–588, 2003.

[29] H. Ismail, S. Z. Salleh, and Z. Ahmad, "Properties of halloysite nanotube (HNT) filled SMR L and ENR 50 nanocomposites," *International Journal of Polymeric Materials and Polymeric Biomaterials*, vol. 62, no. 6, pp. 314–322, 2013.